

Theoretical studies of electronic and crystal structure properties of anhydrous mercury oxalate

A. Koleżyński · A. Małecki

CCTA10 Special Issue
© Akadémiai Kiadó, Budapest, Hungary 2010

Abstract The results of theoretical analysis of the crystal structure and bonding in relation to thermal decomposition process in anhydrous mercury oxalate are presented. The methods used Bader's Quantum Theory of Atoms in Molecules formalism with bond order model (by Cioslowski and Mixon), applied to electron density obtained from ab initio calculations carried out with FP-LAPW Wien2k package (Full Potential Linearized Augmented Plane Wave Method) and Brown's Bond Valence Model are described. The analysis of the obtained results shows that most probably the thermal decomposition process of mercury oxalate should lead to metal and CO₂ as products (as it is experimentally observed). Presented results (as well as the results of our similar calculations carried out previously for zinc, cadmium silver, cobalt and calcium oxalates) allow us to state that such methods (topological and structural), used simultaneously in analysis of the crystal structure and bonding properties, provide us with the additional insight into given compound's behavior during thermal decomposition process. As a result, these methods can be considered as valuable supporting tool in the analysis of thermal decomposition process in given compound.

Keywords Bond order · Bond strength · Bond valence · Electron density topology · FP-LAPW DFT calculations · Thermal decomposition of oxalates

Introduction

Anhydrous bivalent metal oxalates MC₂O₄ form an interesting group of compounds with very similar layered crystal structures (monoclinic unit cell) and well-defined oxalate anions surrounded by metallic cations, but different pathways of thermal decomposition process (M + CO₂, MO + CO + CO₂ or MCO₃ + CO [1–10]).

Despite many experimental results available, there is still lack of consistent theoretical description and explanation of the pathways of thermal decomposition of these compounds. It can be expected, however, that the key role in thermal decomposition process plays the properties of electronic structure and chemical bonding (which in turn due to the structural similarities depend mainly on the characteristic properties of metallic cation). Thus, theoretical studies of fundamental features of electron density (topological analysis) and chemical bonding (bond order, bond valence, bond strains, etc.) carried out for this group of compounds should in principle allow to explain and predict the pathway of thermal decomposition process in given compound (or at least shed some light on the relations between their electronic and crystal structure and bonding properties and pathway of thermal decomposition process).

Recently in a series of papers [11–15], we have proposed theoretical approach, based on the topological analysis of electron density (Bader's Quantum Theory of Atoms in Molecules [16] formalism) obtained from first principles FP-LAPW calculations and structural and bonding properties—bond valence, bond strength, and stresses associated with deviation of given structure from ideal one (Brown's Bond Valence Method [17] founded on Pauling's “electrostatic valence rule” [18]). As our previous results suggest, such approach can give us the additional insight into the

A. Koleżyński (✉) · A. Małecki
Faculty of Materials Science and Ceramics, AGH University
of Science and Technology, Al. Mickiewicza 30,
30-059 Kraków, Poland
e-mail: andrzej.kolezynski@agh.edu.pl

thermal decomposition process and help not only to explain thermal decomposition path in given oxalate, but also—to some extent—to predict such most probably path for the compounds for which experimental results are unavailable.

In this article, the results of similar analysis carried out for anhydrous mercury(II) oxalate HgC_2O_4 are presented (detailed description of methods used here has been presented in our previous papers [11–15]).

Computational details

The electronic structure calculations for anhydrous mercury oxalate have been performed using WIEN2k FP-LAPW (Full Potential Linearized Augmented Plane Wave Method) package [19], within density functional theory (DFT) formalism [20–25]. The following parameters have been used in calculations: 200 k-points ($6 \times 5 \times 5$ mesh within the irreducible Brillouin zone), cut-off parameter $Rk_{\max} = 7.5$, GGA-PBE exchange–correlation potential [26], the values of muffin-tin radii (R_i) [au]: M: 1.8, O: 1.17, C: 1.17 and the convergence criteria for SCF calculations set to $\Delta E_{\text{SCF}} \leq 10^{-5} \text{Ry}$ for total energy and $\Delta \rho_{\text{SCF}} \leq 10^{-5} \text{e} \cdot \text{au}^{-3}$ for electron density topology analysis. The crystal structure parameters and fractional atomic coordinates used in calculations are listed in Table 1.

Crystal structure of anhydrous mercury oxalate

The crystal structure of anhydrous mercury(II) oxalate [27] is formed by layers of edge sharing distorted cubes (each one consists of mercury atom surrounded by eight oxygen atoms) lying in xz plane (Fig. 1c) connected via oxalate anions along y -direction (Fig. 1a, b). One can also analyze the structure from the oxalate environment point of view: every oxalate anion is surrounded by six mercury atoms—two groups of three atoms from neighboring planes (Fig. 2a, b).

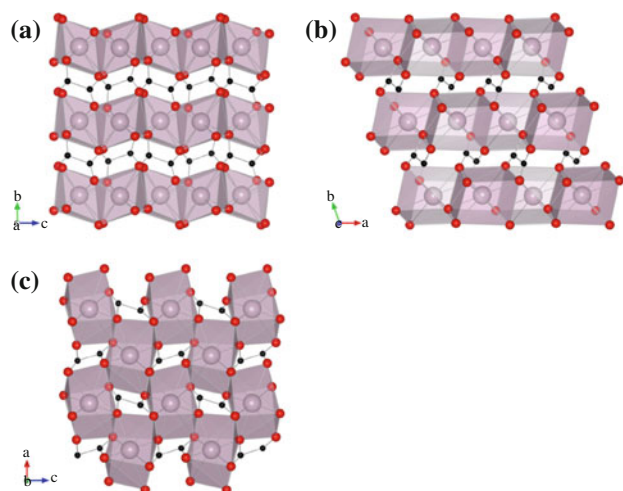


Fig. 1 Anhydrous mercury oxalate crystal structure projected onto yz , xy , and xz planes. All crystal structure figures have been prepared with VESTA visualization software [28]

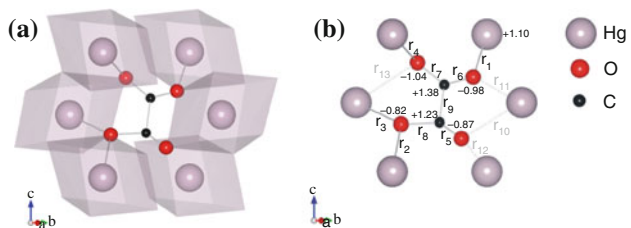


Fig. 2 **a** Oxalate anion environment in anhydrous mercury(II) oxalate. Respective bond lengths are presented in Table 2. The values of AIM total charges calculated for pseudoatoms are presented close to respective atoms (**b**)

Results

The total electron density distribution data obtained from FP-LAPW SCF calculations has been used as a basis for Bader's Quantum Theory of Atoms in Molecules [16] analysis of electron density topology. As Bader et al. [29]

Table 1 Anhydrous mercury(II) oxalate crystal structure data [27]

| Structure | Space group | a/Å | b/Å | c/Å | $\beta/^\circ$ | V/Å³ | | | |
|-------------------------------|-------------------------|-----------|-----------|------------------|----------------|--------|--------|--------|------------------|
| CaC2O4 | P2 ₁ (No. 4) | 5.029 (1) | 5.228 (1) | 6.437 (1) | 108.82 (1) | 160.19 | | | |
| Fractional atomic coordinates | | | | | | | | | |
| Atom | x | y | z | Wyckoff position | Atom | x | y | z | Wyckoff position |
| Hg | 0.5060 | 0.2500 | 0.2470 | 2a | O1 | 0.8740 | 0.0420 | 0.1110 | 2a |
| C1 | 0.0680 | 0.8800 | 0.2290 | 2a | O2 | 0.2980 | 0.9370 | 0.3310 | 2a |
| C2 | 0.9620 | 0.6070 | 0.3040 | 2a | O3 | 0.6790 | 0.5940 | 0.1390 | 2a |
| | | | | | O4 | 0.1040 | 0.4910 | 0.4220 | 2a |

Table 2 Bond lengths R_{AB} and BCP parameters: Hessian eigenvalues $\lambda_1-\lambda_3$, electron density ρ_{BCP} , Laplacian $\nabla^2\rho(r)$, potential energy density $V(r)$, and electronic energy density $H_e(r)$, calculated for anhydrous mercury(II) oxalate

| HgC_2O_4 | $R_{AB}/\text{\AA}$ | $\lambda_1/\text{e au}^{-5}$ | $\lambda_2/\text{e au}^{-5}$ | $\lambda_3/\text{e au}^{-5}$ | $\rho_{BCP}/\text{e au}^{-3}$ | $\nabla^2\rho(r)/\text{e au}^{-5}$ | $V(r)/\text{Ry au}^{-3}$ | $H_e(r)/\text{Ry au}^{-3}$ |
|---|---------------------|------------------------------|------------------------------|------------------------------|-------------------------------|------------------------------------|--------------------------|----------------------------|
| r_1 (Hg–O ₂) | 2.105 | −0.1363 | −0.1328 | 0.6369 | 0.1012 | 0.3678 | −0.8610 | −0.3845 |
| r_2 (Hg–O _{3a}) | 2.206 | −0.1060 | −0.1040 | 0.4621 | 0.0862 | 0.2521 | −0.7199 | −0.3284 |
| r_3 (Hg–O _{3b}) | 2.493 | −0.0433 | −0.0416 | 0.2383 | 0.0403 | 0.1535 | −0.2127 | −0.0872 |
| r_4 (Hg–O ₁) | 2.534 | −0.0377 | −0.0357 | 0.2089 | 0.0374 | 0.1355 | −0.1724 | −0.0693 |
| r_5 (C ₂ –O ₄) | 1.051 | −2.2000 | −2.1020 | 6.0350 | 0.6119 | 1.7340 | −2.5237 | −1.0451 |
| r_6 (C ₁ –O ₂) | 1.170 | −1.3540 | −1.3210 | 3.0000 | 0.4549 | 0.3248 | −2.0050 | −0.9619 |
| r_7 (C ₁ –O ₁) | 1.330 | −0.7639 | −0.6999 | 0.7015 | 0.3344 | −0.7624 | −1.2465 | −0.7186 |
| r_8 (C ₂ –O ₃) | 1.477 | −0.5028 | −0.4708 | 0.4506 | 0.2460 | −0.5230 | −2.3366 | −1.2337 |
| r_9 (C ₁ –C ₂) | 1.649 | −0.3965 | −0.3592 | 0.3722 | 0.2033 | −0.3836 | −1.6316 | −0.8638 |

have shown, the gradient vector field, derived from the scalar electron density distribution allows one to separate uniquely the total electron density by means of zero flux surfaces into non-overlapping, pseudoatomic subsystems of the whole many electron many nuclear system, containing a single nucleus (such pseudoatoms possess very important feature: the expected value of any observed quantity described by a Hermitian operator \hat{A} for the whole system can be presented as a sum of pseudoatomic contributions $\langle \hat{A} \rangle = \sum_i \hat{A}(\Omega_i)$, regardless of whether \hat{A} is a one-electron or a many electron operator). What is more, Bader has pointed out the important role of electron density gradient $\nabla\rho(r)$ and Laplacian $\nabla^2\rho(r)$ —the topological properties of electron density are revealed in the analysis of the corresponding gradient field and important features of ρ are described by critical points r_{CP} at which $\nabla\rho(r_{CP}) = 0$ (we constrained ourselves in our present analysis to bond critical points only), while Laplacian provides important information about the character of electron density distribution in both, bonding and non-bonding regions [30] ($\nabla^2\rho(r)$ measures electron density concentration $\nabla^2\rho(r) < 0$ or depletion $\nabla^2\rho(r) > 0$ in given region). He has also introduced an important characteristic of bonding in many-electron many-nuclear system—the local electron energy $H_e(r) = G(r) + V(r)$, which can be expressed in terms of electrostatic potential, electron density, and its Laplacian by the formula $H_e(r) = 1/2[V(r) + 1/4\nabla^2\rho(r)]$. The sign of $H_e(r)$ uniquely indicates whether the kinetic or potential energy dominates in given region in space—negative value of $H_e(r)$ means that the potential energy dominates and the accumulation of electrons is stabilizing in this region of space (thus the condition $\nabla^2\rho(r) > 0$ in the inter-nuclear space is not sufficient for system to become unbounded, since the electron energy $H_e(r)$ can still be negative in case of sufficiently strong electrostatic potential here [31]).

Such topological analysis of electron density has been carried out for anhydrous mercury(II) oxalate, and the results obtained for bond critical points are presented in

Table 2. Characteristic parameters of BCPs have been in turn used as a basis for the calculations of bond orders. As in our previous calculations [11–15], the bond order formula proposed by Cioslowski and Mixon [32] (in an improved form suggested by Howard and Lamarche [33]) has been used here. The respective bond orders calculated for anhydrous mercury oxalate are presented in Table 3.

Additional and complementary information about the bonding properties has been obtained from experimental crystal structure data using Bond Valence Method proposed by Brown [17]. This method not only gives us information about the atomic and bond valences (which can be related to bond strength and thus to bond order), but also allows us to estimate the values of the strains acting on single bonds as well as the overall strains present in given structure. There are two different types of indicators of such stresses: d_i and D measuring, respectively, the level of deviation of given atom environment or entire crystal structure from ideal one and strain factor δ providing information about the strains acting on single bonds or groups of bonds [see details in [11, 12]]. The values of bond valences s_{ij} and bond strain factors calculated from structural data for anhydrous mercury(II) oxalate are presented in Table 4 (only bond valences and bond strain

Table 3 Bond orders calculated from topological properties of electron density in bond critical points for anhydrous mercury(II) oxalate

| Bond no. | $n_{CM(HL)}$ | Bond no. | $n_{CM(HL)}$ |
|-----------------------------|--------------|---|--------------|
| r_1 (Hg–O ₂) | 0.95 | r_5 (C ₂ –O ₄) | 2.39 |
| r_2 (Hg–O _{3a}) | 0.90 | r_6 (C ₁ –O ₂) | 1.58 |
| r_3 (Hg–O _{3b}) | 0.84 | r_7 (C ₁ –O ₁) | 0.96 |
| r_4 (Hg–O ₁) | 0.83 | r_8 (C ₂ –O ₃) | 0.90 |
| | | r_9 (C ₁ –C ₂) | 0.57 |

Table 4 Bond lengths and bond valences (theoretical and experimental ones) and bond strain factors calculated for anhydrous mercury(II) oxalates (see text for details)

| HgC ₂ O ₄ | $R_{\text{theor}}/\text{\AA}$ | $R_{\text{exp}}/\text{\AA}$ | s_{ij}^{theor} | s_{ij}^{exp} | δ | | | |
|---|-------------------------------|-----------------------------|-------------------------|-----------------------|--------------------------|--------|--------------------------------|--------|
| r_1 (Hg–O ₂) | 2.228 | 2.105 | ½ | 0.6989 | $\delta_{\text{Hg–O}}$ | 0.2148 | $\delta_{\text{Hg–O}_2}$ | 0.1989 |
| r_2 (Hg–O _{3a}) | 2.228 | 2.206 | ½ | 0.5318 | | | $\delta_{\text{Hg–O}_{3a}}$ | 0.0318 |
| r_3 (Hg–O _{3b}) | 2.228 | 2.493 | ½ | 0.2449 | | | $\delta_{\text{Hg–O}_{3b}}$ | 0.2551 |
| r_4 (Hg–O ₁) | 2.228 | 2.534 | ½ | 0.2192 | | | $\delta_{\text{Hg–O}_1}$ | 0.2808 |
| r_5 (C ₂ –O ₄) | 1.134 | 1.051 | 2 | 2.4994 | $\delta_{\text{C–O}}$ | 0.3525 | $\delta_{\text{C}_2–\text{O}}$ | 0.4994 |
| r_6 (C ₁ –O ₂) | 1.240 | 1.170 | 1½ | 1.8146 | | | $\delta_{\text{C}_1–\text{O}}$ | 0.3146 |
| r_7 (C ₁ –O ₁) | 1.240 | 1.330 | 1½ | 1.1772 | $\delta_{\text{C–C}}$ | 0.2559 | | |
| r_8 (C ₂ –O ₃) | 1.390 | 1.477 | 1 | 0.7894 | δ_{Struct} | 0.2881 | | |
| r_9 (C ₁ –C ₂) | 1.540 | 1.649 | 1 | 0.7441 | | | | |

factors are presented here, since they are directly related to bond properties and thus are important for our analysis).

The following equations (formulated with the aid of BCPs found during the topological analysis of electron density) have been used for theoretical valences calculation in anhydrous mercury oxalate, according to Valence Sum Rule:

$$\text{Hg} = r_1 + r_2 + r_3 + r_4 = 1/2 + 1/2 + 1/2 + 1/2 = 2$$

$$\text{C}_1 = r_6 + r_7 + r_9 = 1/2 + 1/2 + 1 = 4$$

$$\text{C}_2 = r_5 + r_8 + r_9 = 2 + 1 + 1 = 4$$

$$\text{O}_1 = r_4 + r_7 = 1/2 + 1/2 = 2$$

$$\text{O}_2 = r_1 + r_6 = 1/2 + 1/2 = 2$$

$$\text{O}_3 = r_2 + r_3 + r_8 = 1/2 + 1/2 + 1 = 2$$

$$\text{O}_4 = r_5 = 2.$$

Discussion

The results of topological analysis (Table 2) show that first of all we have only nine different bond types in a system and some of mercury atoms neighboring oxalate anion are not bonded with respective oxygen atoms (gray dotted lines on Fig. 2b, denoted from r_{10} to r_{13}). Next, we can see that all mercury–oxygen bonds exhibit weak ionic character (positive value of Laplacian in respective BCPs), while carbon–carbon bonds have strong covalent character ($\nabla^2(\rho) < 0$). The carbon–oxide bonds fall into two sets of two similar bonds: r_5 and r_6 exhibit strong and weak ionic character, respectively, while r_7 and r_8 have strong covalent character. These results are quite typical for oxalates [11–15], except for the bonds r_5 and r_6 , since carbon–oxide bonds have usually dominating covalent character. However, careful analysis of the values of potential and electronic energy density in bond region shows clearly that potential energy dominates over the kinetic energy here and overall electronic energy is negative and thus these bonds are energetically stable. The bond orders calculated from BCP parameters (Table 3) suggest that the weakest

bonds in anhydrous mercury oxalate crystal are those created between carbon atoms within oxalate groups (r_9), while Hg–O bonds (r_1 – r_4) are much stronger. Similarly, as in case of BCP properties, carbon–oxide bonds form two sets, two bonds (r_7 – r_8), have similar strength as Hg–O bonds and two are significantly stronger (r_5 – r_6).

Additional insight into the bonding properties in anhydrous mercury(II) oxalate can be obtained from Table 4. It is quite evident—according to calculated strain factors δ —that the entire structure is far from ideal one and there are strong forces acting on all bonds (the bond lengths calculated from theoretical bond valences deviate strongly from experimental ones—two mercury bonds r_1 and r_2 are too short while the other two r_3 and r_4 are too long; similarly two carbon–oxide bonds r_5 and r_6 are too short and r_7 and r_8 are too long and finally C–C bond r_9 is too long), which means, that all bonds are strained, compressed, or stretched and thus will exhibit the tendency to lengthen or to shorten, respectively, during bond breaking in thermal decomposition process.

The obtained results allow us to propose the most probable pathway of thermal decomposition process in anhydrous mercury oxalate. Since C–C bond is the weakest one, it should break as the first one. This will result in immediate charge flow mainly to C–O bonds (and to some extent probably also to Hg–O bonds). It is convenient to analyze the next steps of bond breaking process separately for groups of bond created by individual oxygen atoms. In case of O₁ atom (bonds r_4 and r_7), both bonds are too long and will tend to shorten (r_7 bond slightly more due to larger tensile stress). This will result in bonds strengthening, but again to greater extent in case of r_7 bond and therefore most likely the r_4 bond will break here. For O₂ atom, we have two compressed bonds (r_1 and r_6), so after C–C bond breaking, these bonds will tend to lengthen and will become weaker. Since carbon–oxygen bond (r_6) is much stronger, despite the stronger compression and thus probably stronger weakening during elongation, mercury–

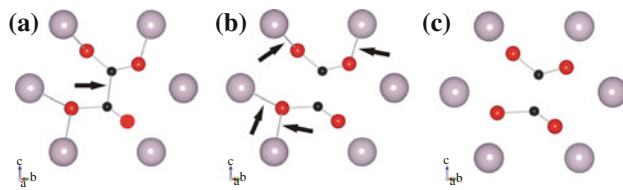


Fig. 3 Bond breaking sequence in anhydrous mercury(II) oxalate

oxygen bond (r_1) will remain much weaker and thus this is the one which should break here. The situation in last case (O_3 atom) is as follows: according to topological analysis (the existence of BCPs), oxygen atom form three bonds, one with carbon (r_8) and two with mercury (r_2 and r_3). Bonds r_3 and r_8 are stretched and will tend to shorten which will result in their strengthening and bond r_2 will shorten only slightly due to very small compressive strains. Consequently, since the tensile strains acting on bonds r_3 and r_8 are of similar magnitude, the latter one will remain stronger and we can expect that at this stage of thermal decomposition process, both mercury–oxygen bonds should break and carbon–oxide bond (r_8) should be preserved. The last oxygen atom (O_4) form only one bond with carbon and this bond should be preserved with slightly changed length and strength.

Ultimately, as a result of described above consecutive steps of bond breaking during thermal decomposition process, we will obtain metallic mercury and carbon dioxide as the products (Fig. 3), in agreement with the experiment [34, 35].

Summary

The main purpose of this article was the application of previously proposed theoretical approach, based on joint analysis of the electron density topology and structural data, to the description and explanation of the crystal structure and bonding properties in anhydrous mercury(II) oxalate and their relations with thermal decomposition process, leading in this case to metal and carbon dioxide as products. Presented results allowed us to propose the most probable sequence of bond breaking during the thermal decomposition process (in agreement with the experiment). In the light of this results as well as our previous investigations of electronic and crystal structure and bonding properties carried out for series of anhydrous oxalates, we are convinced that despite the obvious limitations of quantum mechanical approach to chemistry (due to necessary approximations and idealizations inherent in all quantum methods in solid state) the proposed approach can be considered as valuable additional tool in the analysis of thermal decomposition process in given compound

(especially that it is based mainly on the modern topological analysis of electron density which allow to reinstate the very chemical concept of atoms in molecules and bonds—the concepts which are simply missing in classical quantum mechanical approach based on wave function).

Acknowledgements This study has been supported by AGH-UST grant no 11.11.160.110.

References

- Malecka B, Drożdż-Cieśla E, Małecki A. Mechanism and kinetics of thermal decomposition of zinc oxalate. *Thermochim Acta*. 2004;423:13–8.
- Brown ME, Dollimore D, Galwey AK. Comprehensive chemical kinetics. In: Bamford CH, Tipper CFH, editors. *Reactions in solid state*, vol. 2. Amsterdam: Elsevier; 1980.
- Boldyrev VV, Nevyantsev IS, Mikhailov YI, Khayretdinov EF. K voprosu o myekhanizme tyermicheskogo razlozheniya oksalatov. *Kinet Katal*. 1970;11:367–73.
- Borchardt HJ, Daniels F. The application of differential thermal analysis to the study of reaction kinetics. *J Am Chem Soc*. 1957;79:41–6.
- Dollimore D. The thermal decomposition of oxalates. A review. *Thermochim Acta*. 1987;117:331–63.
- Randhawa BS, Kaur M. A comparative study on the thermal decomposition of some transition metal maleates and fumarates. *J Therm Anal Calorim*. 2007;89(1):251–5.
- Galwey AK, Brown ME. An appreciation of the chemical approach of V. V. Boldyrev to the study of the decomposition of solids. *J Therm Anal Calorim*. 2007;90(1):9–22.
- Fujita J, Nakamoto K, Kobayashi M. Infrared spectra of metallic complexes. III. The infrared spectra of metallic oxalates. *J Phys Chem*. 1957;61(7):1014–5.
- Rane S, Uskaikar H, Pednekar R, Mhalsikar R. The low temperature synthesis of metal oxides by novel hydrazine method. *J Therm Anal Calorim*. 2007;90(3):627–38.
- Bîrzescu M, Niculescu M, Dumitru Raluca, Carp Oana, Segal E. Synthesis, structural characterization and thermal analysis of the cobalt(II) oxalate obtained through the reaction of 1,2-ethanediol with $Co(NO_3)_2 \cdot 6H_2O$. *J Therm Anal Calorim*. 2009;96(3):979–86.
- Koleżyński A, Małecki A. Theoretical studies of thermal decomposition of anhydrous cadmium and silver oxalates. Part I. Electronic structure calculations. *J Therm Anal Calorim*. 2009;96(1):161–5.
- Koleżyński A, Małecki A. Theoretical studies of thermal decomposition of anhydrous cadmium and silver oxalates. Part II. Correlations between the electronic structure and the ways of thermal decomposition. *J Therm Anal Calorim*. 2009;96(1):167–73.
- Koleżyński A, Małecki A. First principles studies of thermal decomposition of anhydrous zinc oxalate. *J Therm Anal Calorim*. 2009;96(2):645–51.
- Koleżyński A, Małecki A. Theoretical approach to thermal decomposition process of chosen anhydrous oxalates. *J Therm Anal Calorim*. 2009;97(1):77–83.
- Koleżyński A, Małecki A. Theoretical analysis of electronic and structural properties of anhydrous calcium oxalate. *J Therm Anal Calorim*. 2010;99(3):947–55.
- Bader RFW. *Atoms in molecules: a quantum theory*. Oxford: Clarendon Press; 1990.

17. Brown ID. The chemical bond in inorganic chemistry. The bond valence model. Oxford: Oxford University Press; 2002.
18. Pauling L. The principles determining the structure of complex ionic crystals. *J Am Chem Soc.* 1929;51:1010–26.
19. Blaha P, Schwarz K, Madsen GKH, Kvasnicka D, Luitz J. WIEN2k. An augmented plane wave + local orbitals program for calculating crystal properties. Wien: Karlheinz Schwarz, Techn. Universität Wien; 2001. ISBN 3-9501031-1-2
20. Slater JC. Wave functions in a periodic potential. *Phys Rev.* 1937;51(10):846–51.
21. Loucks TL. Augmented plane wave method. New York: Benjamin; 1967.
22. Andersen OK. Simple approach to the band-structure problem. *Solid State Comm.* 1973;13(2):133–6.
23. Hamann DR. Semiconductor charge densities with hard-core and soft-core pseudopotentials. *Phys Rev Lett.* 1979;42(10):662–5.
24. Wimmer E, Krakauer H, Weinert M, Freeman AJ. Full-potential self-consistent linearized-augmented-plane-wave method for calculating the electronic structure of molecules and surfaces: O₂ molecule. *Phys Rev B.* 1981;24(2):864–75.
25. Singh DJ. Planewaves, pseudopotentials and the LAPW method. Dordrecht: Kluwer Academic Publishers; 1994.
26. Perdew JP, Burke K, Ernzerhof M. Generalized gradient approximation made simple. *Phys Rev Lett.* 1996;77(18):3865–8.
27. Christensen AN, Norby P, Hanson JC. A crystal structure determination of Hg C₂ O₄ from synchrotron X-ray and neutron powder diffraction data. *Z Kristallogr.* 1994;209:874–7.
28. Momma K, Izumi F. VESTA: a three-dimensional visualization system for electronic and structural analysis. *J Appl Crystallogr.* 2008;41(3):653–8.
29. Bader RFW, Slee TS, Cremer D, Kraka E. Description of conjugation and hyperconjugation in terms of electron distributions. *J Am Chem Soc.* 1983;105(15):5061–8.
30. Bader RFW, Essen H. The characterization of atomic interactions. *J Chem Phys.* 1984;80:1943–60.
31. Tsirelson VG, Ozerov RP. Electron density and bonding in crystals. Principles, theory and X-ray diffraction Experiments in solid state physics and chemistry. Bristol, Philadelphia: IOP Publishing Ltd; 1996.
32. Cioslowski J, Mixon ST. Covalent bond orders in the topological theory of atoms in molecules. *J Am Chem Soc.* 1991;113(11): 4142–5.
33. Howard ST, Lamarche O. Description of covalent bond orders using the charge density topology. *J Phys Org Chem.* 2003;16(2): 133–41.
34. Lvov BV. Kinetics and mechanism of thermal decomposition of nickel, manganese, silver, mercury and lead oxalates. *Thermochim Acta.* 2000;364:99–109.
35. Lvov, BL. Thermal decomposition of solids and melts. New thermochemical approach to the mechanism, kinetics and methodology. Netherland: Springer; 2007.